This article has been accepted for publication in a future issue of this journal, but has not been fully edited. Content may change prior to final publication. Citation information: DOI 10.1109/LAWP.2018.2878950, IEEE Antennas and Wireless Propagation Letters

In-body and Off-body Channel Modeling for Future Leadless Cardiac Pacemakers based on Phantom and Animal Experiments

Pritam Bose, Ali Khaleghi, *Senior Member, IEEE*, Ilangko Balasingham, *Senior Member, IEEE*

***Abstract*— In this letter, the in-body and off-body channel models at the frequency of 2.4 GHz are studied for development of multi-node leadless capsule pacemaker technology based on experiments in homogeneous liquid phantom model of human heart and living animal experiments. For conducting the experiments, we design a battery-operated self-contained transmitter capsule consisting of a small antenna and transmitter printed-circuit board, sub-cutaneous implant and the off-body antennas. The in-body path-loss model obtained from the phantom experiment is a linear function of distance, whereas the off-body path-loss model between the implant and the off-body antenna is a logarithmic function of distance comparable to the free-space path-loss model. The phantom experiment study shows that coupling between implants decreases linearly at the rate of 3.6 dB/cm for cardiac implants and by 4.1 dB/cm for cardiac to sub-cutaneous implant at 2.4 GHz. The animal experiment results are in good accordance with the phantom results.**

I. INTRODUCTION

Leadless cardiac pacemaker is an innovative technology that can be a replacement to the widely used pacemaker technology with leads [1]. There are currently two commercially available leadless pacing systems: the Nanostim leadless cardiac pacemaker (LCP) device (St. Jude Medical, Sylmar, California) [2] and the Micra Transcatheter pacing system (TPS) (Medtronic, Minneapolis, Minnesota) [3]. Both these technologies offer single-chamber stimulation but the technology providing multi-chamber stimulations and cardiac resynchronization will be an optimum solution [4]. Recent research introduces the multi-nodal leadless pacemaker technology where each unit will hereinafter be called capsules (see Fig. 1). All the capsules will be equipped with radio-frequency (RF) communication module to develop a sensor network. To build the RF communication network, the in-body channel models inside the heart and surrounding the heart need to be clearly understood. To the best of our knowledge, very little research has been done to characterize the in-body channel models [5, 6]. Moreover, the channel models vary depending on the position of the implant inside the body and with the frequency of operation.

This work was funded by the European Union's H2020: MSCA: ITN program for the "Wireless In-body Environment Communication – WiBEC" project under the grant agreement no. 675353.

Pritam Bose is with the Intervention Center, Oslo University Hospital, NO-0027 Oslo and also with the Faculty of Medicine, University of Oslo, 0315, Oslo, Norway (e-mail: pritam.bose@studmed.uio.no).

Ali Khaleghi and Ilangko Balasingham are with the Intervention Center, Oslo University Hospital, NO-0027 Oslo and with the Department of Electronic Systems, Norwegian University of Science and Technology, 7491 Trondheim, Norway (e-mail: ali.khaleghi@ntnu.no and ilangko.balasingham@medisin.uio.no).

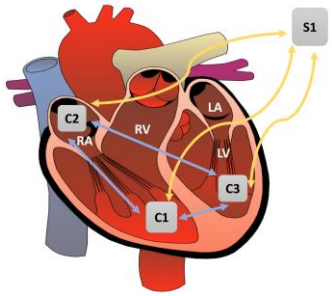

Fig. 1 Schematic of a three-node leadless capsule pacemaker application for cardiac resynchronization therapy. The capsules C1, C2 and C3 are placed inside the chambers of the heart and they can communicate with the subcutaneous implant S1. RA- right atrium, RV- right ventricle, LA- left atrium, LV- left ventricle, C- capsules and S- subcutaneous implant.

The body is a heterogeneous medium consisting of frequency dependent lossy tissues having different permittivity and conductivity. Tissues such as blood and muscle having high water content and minerals, cause more attenuation of RF signals compared to fat or bone with low water content. The research focuses on developing the channel model for cardiac implant to implant communication and cardiac implant to sub-cutaneous implant communication using phantom and living animal experiments. The channel models are obtained at Industrial, Scientific and Medical (ISM) band at 2.4 GHz. The frequency selection is done because of easy implementation of a very small antenna providing reasonable radiation efficiency and matching, as reported in [7]. In addition, the possibility of decreasing the physical size of the antenna and the embedded electronics provides us more space for a larger sized battery, thereby increasing the lifetime of the pacemaker device.

The paper is organized as follows: Section II describes the components fabricated for the study. Phantom and living animal experimental setups are shown in Section III followed by description of experimental results in Section IV. Finally, concluding remarks and future directions are expressed in Section V.

II. FABRICATED COMPONENTS

A simple encapsulated transmitter is designed and fabricated on a printed circuit board (PCB). The capsule includes a transmitter source, a matched antenna, battery resources and a plastic shell (see Fig 2a). The PCB contains a voltage-controlled oscillator (VCO) IC (HMC385LP4E) operating at 3V and generating a sinusoidal signal at 2.4 GHz. The implant antenna has a meander shape with almost dual polar radiation pattern due to the meander line orientations in both the vertical and horizontal paths [8]. The meander line geometry increases the electrical length of the antenna for miniaturization. Capacitive coupling mechanism

1536-1225 (c) 2018 IEEE. Personal use is permitted, but republication/redistribution requires IEEE permission. See http://www.ieee.org/publications_standards/publications/rights/index.html for more information.

This article has been accepted for publication in a future issue of this journal, but has not been fully edited. Content may change prior to final publication. Citation information: DOI 10.1109/LAWP.2018.2878950, IEEE Antennas and Wireless Propagation Letters

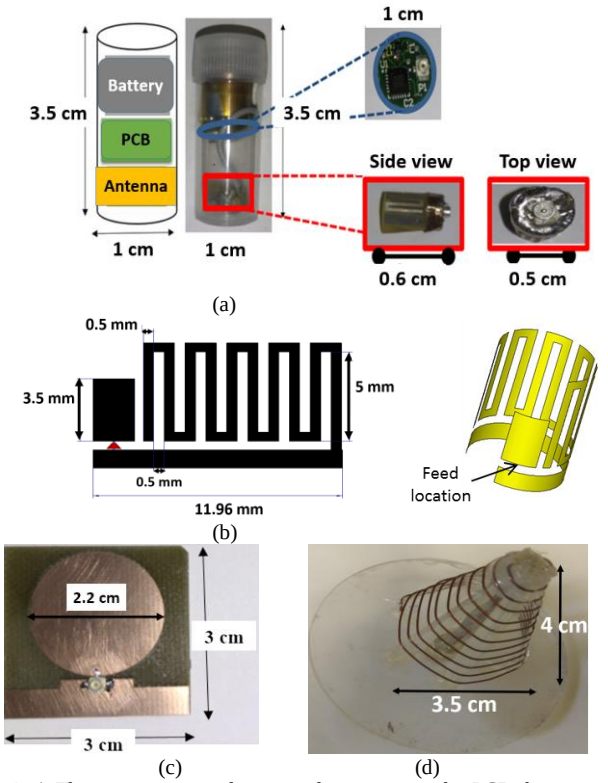

Fig. 2 a) The transmitter implant capsule containing the PCB, battery and meander antenna b) the planar meander antenna geometry and the conformal antenna c) sub-cutaneous implant patch antenna d) Off-body spiral antenna

is used for the meander section feeding to generate resonance frequency with a tunable input resistance [9]. The planar antenna is printed on a flexible substrate material and has a cylindrical conformal geometry to reduce the space and simplify the integration in a cardiac capsule. The planar antenna dimensions are shown in Fig. 2b. The conformal cylinder shape antenna has an operating frequency of 2.4 GHz which is matched to the signal source with 50-ohm impedance when embedded in a sample heart tissue. The simulated S11 is below -10 dB with 40 MHz of the operating bandwidth.

We have used a waterproof plastic shell to seal the electronics and antenna from direct contact with the liquid phantom and in-vivo tissues. The shell thickness is 0.5 mm and there is a 2 mm air gap around the antenna to limit the direct power coupling to the lossy medium for reducing the material loss and increasing the radiation efficiency. The measured S11 is about -11 dB at 2.4 GHz when encapsulated in a plastic shell and placed inside the liquid phantom. The antenna provides 80 MHz of the bandwidth due to more loss caused by the antenna installations. We note that the measurement of such small antennas using cables cannot be very accurate, but we estimate that the antenna is well matched to the source impedance. The current coupling on the cables increases the antenna physical length and causes uncertainty with impedance readings and resonance frequency. The measurements with ferrite beads on the cable can lead to more accurate reading but the ferrite beads at 2.4 GHz are not effective. There are appropriate for the frequencies below 1 GHz. We have used a non-conventional approach for estimating the antenna resonance and operating frequency. We have integrated a pulse generator with 1 MHz repetition frequency within the antenna structure (instead of the 2.4 GHz transmitter). The spectrum is very wide and covers the frequencies from 1 MHz up to 3.5 GHz. The signal feeds the implant antenna and an ultra-wide band receiver antenna at about 2 GHz, which is used to monitor the radiation spectrum. It is observed that the radiation spectrum is maximum at about 2.4 GHz and decays sharply away from it, which proves the best matching at 2.4 GHz frequency band. In addition, the EM simulations of the antenna structure is a proof for the antenna operation at 2.4 GHz. In general, we can observe that the antenna radiation is maximum at 2.4 GHz, but we cannot provide the exact impedance of the antenna at that frequency as we don't have access to the reflected antenna signal. The radiation pattern of the embedded antenna is evaluated via EM simulations. The embedded antenna proves dual polar radiation pattern.

The sub-cutaneous implant antenna (Fig. 2c) is a wide-band patch antenna of dimensions 3×3 cm^2 which is the receiver antenna and has a wideband impedance matching. It is a monopole like antenna with linear polarization in which the antenna orientation is adjusted during the experiment to observe maximum received signal level. The patch antenna can operate in the frequency band of 1.6 GHz to 3.2 GHz with S11< -11 dB at 2.4 GHz when covered in a thin plastic layer and placed inside the liquid phantom.

The off-body spiral antenna (see Fig. 2d) is a wideband circular polarized antenna with two orthogonal polarizations and the antenna on-axis orientation has minor effect on the signal level [10]. The antenna provides high gain (about 9 dBi) and directive pattern in the apex direction, thus high field intensity in its broadside direction is generated. The antenna is used for the wireless link measurement in distance from the body surface.

III. Phantom Setup and Living Animal Experiments

The initial experiments are done in a phantom model to determine the in-body channel models for cardiac implant to implant communications. Our phantom model is a 39.2% homogeneous sucrose solution that mimics the permittivity and conductivity of human heart at 2.4 GHz [11]. The liquid phantom is stored in a plastic container of size 24×30×30 cm^3. The transmitter capsule is placed inside the liquid phantom by attaching to a plastic rod to hold the antenna during the measurements. The receiver patch antenna is encapsulated inside a thin plastic layer to prevent direct contact with the liquid and is placed in the liquid container (see Fig. 3a). The receiver patch antenna is connected to a spectrum analyser to record the received signal strength. The transmitter capsule is kept at a minimum distance of 1 cm from the receiver antenna and the distance is increased by 1 cm steps gradually to a maximum distance of 16 cm. Above 16 cm, it is noticed that the received signal strength falls below the receiver noise level. The receiver noise power depends on the spectrum analyzer resolution bandwidth. We use FHS8 from R&S company for the measurements. By setting the resolution bandwidth of 300 Hz, the noise level at 2.4 GHz is -120 dBm. Therefore, considering 20 dB of the

1536-1225 (c) 2018 IEEE. Personal use is permitted, but republication/redistribution requires IEEE permission. See http://www.ieee.org/publications_standards/publications/rights/index.html for more information.

This article has been accepted for publication in a future issue of this journal, but has not been fully edited. Content may change prior to final publication. Citation information: DOI 10.1109/LAWP.2018.2878950, IEEE Antennas and Wireless Propagation Letters

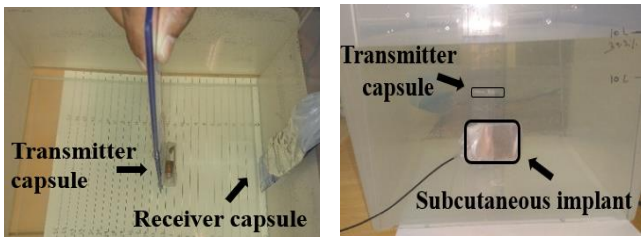

(a) (b)

Fig. 3 Heart phantom solution with a) transmitter and receiver capsules placed inside it and b) transmitter implant capsule placed inside it and the receiver implant placed subcutaneously.

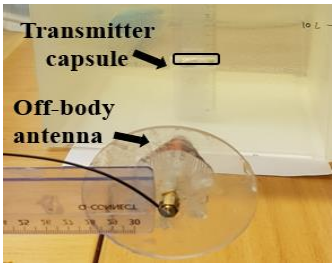

Fig. 4 Heart phantom solution with transmitter implant capsule placed inside it and off-body antenna placed outside the container at varying distances

margin for the measurements, the signal levels above -100 dBm are valid in our experiments.

The second experiment is performed by placing the transmitter capsule inside the phantom solution and the receiver patch antenna subcutaneously on the side of the phantom container (see Fig. 3b). The receiver antenna now behaves like an sub-cutaneous implant antenna. The transmitter capsule is kept at a minimum distance of 1 cm and moved away by 1 cm steps untill a maximum distance of 13 cm. Beyond 13 cm, the recorded signal falls below the noise level.

The final experiment is done by placing the off-body antenna in distance to the container to determine the signal strength outside the phantom from the transmitter capsule (see Fig. 4). This experiment will help us to find the in-body to off-body channel model for determining the risk of evesdropping in the future. The transmitter capsule is placed 10 cm inside the phantom solution from the inner side of the container. The off-body antenna is placed outside the container and is moved from 1 cm till 50 cm. Beyond 50 cm, the received signal strength falls below the receiver noise level. During all the experiments, the transmitter and receiver antennas are aligned on the same plane to have the maximum coupling between them.

The phantoms experiments are followed by living animal measurements to validate the results. The experiments are done on an adult pig weighing 61 kgs. To evaluate and compare the performances of the capsule in an environment similar to that of the human body, the pig used in this experiment is prepared under a general anesthesia. All studies are performed at the hybrid operating room of the Intervention Centre, Rikshospitalet, Oslo University Hospital, Norway that has accreditation for conducting animal experiments. All the experiments are performed in strict compliance with the Norwegian and European Union laws on Ethical standards and humane treatment of animals. Because this animal was alive, and all of its organs were

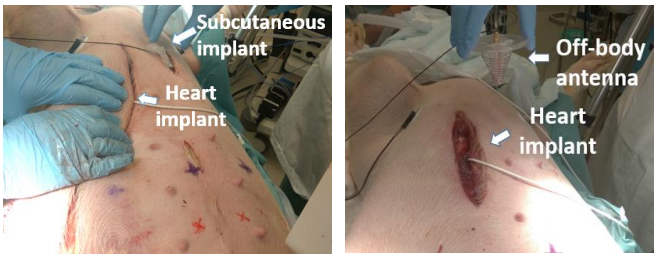

(a) (b)

Fig 5. Photograph showing a) the implant capsule and the sub-cutaneous implant placed surgically inside the pig and) the implant capsule and off-body antenna placed at varying distance outside the pig

operating normally, the experimental conditions were virtually identical to conditions expected in a human body.

The animal measurement setup is equivalent to the previous setup shown in Fig. 3 except that the liquid phantom is replaced in this case by a pig. The experiments to find the coupling for cardiac implant to cardiac implant, cardiac implant to sub-cutaneous implant and cardiac implant to off-body antenna are recorded, respectively. For the cardiac to cardiac implant, the implants are placed on either side of the heart, with one outside the right ventricle and other outside the left atrium (see Fig. 5a). The optimal placement would have been inside the heart chambers, but the heart is not punctured to place the implants inside the heart. This is done to prevent the early death of the animal as it is used for multiple other experiments to increase its usability and reduce the number of animal sacrifices. For the implant to sub-cutaneous implant communication, the implant antenna is placed behind the right ventricle and the sub-cutaneous in the pocket of the shoulder. For the off-body antenna communication, the implant capsule is placed at the same location behind the right ventricle and the off-body is held at multiple distances above the animal (see Fig. 5b). The distance between the implants are measured with the help of a magnetic distance measurement system called Medical Aurora manufactured by the company northern Digital Inc. that gives accurate distance measurements.

IV. MEASUREMENT RESULTS

The cardiac modelling curve was obtained from multiple datasets. We have had taken six measurements at each distance. The spectrum analyzer was put in averaging mode so the results provided in the graph is the average of the values obtained at each distance. This was done to improve the clarity of the figure and make it look less congested. The averaging also removes the small temporal variations of the path loss during the human handling of the setup. The results for the implant to implant communication in the phantom model shows that the coupling varies linearly with distance (see Fig. 6). The path-loss model is given by the following equation:

$$y = A*x + y(1) \qquad (1),$$

where y is the coupling in dB, A is the slope of the equation in dB per cm, x is the distance in cm and y(1) is the maximum coupling at a distance of 1 cm.

The experimental results show that A is -3.6 dB/cm which means that the coupling reduces at a rate of 3.6 dB with

1536-1225 (c) 2018 IEEE. Personal use is permitted, but republication/redistribution requires IEEE permission. See http://www.ieee.org/publications_standards/publications/rights/index.html for more information.

This article has been accepted for publication in a future issue of this journal, but has not been fully edited. Content may change prior to final publication. Citation information: DOI 10.1109/LAWP.2018.2878950, IEEE Antennas and Wireless Propagation Letters

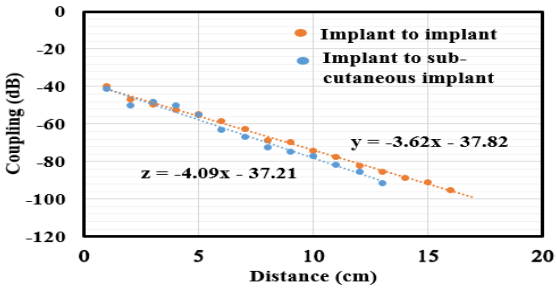

Fig 6. Pathloss model for implant to implant and implant to sub-cutaneous implant communication

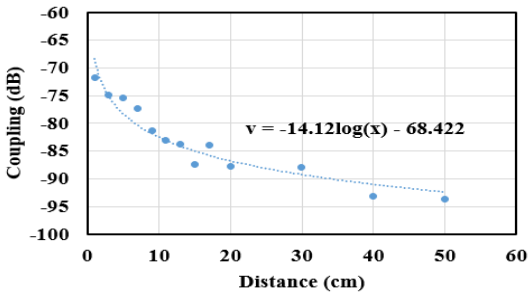

Fig 7. Pathloss model for implant to off-body communication

increase in distance between the implants by each cm. The maximum coupling y(1) is recorded as -37.8 dB.

The coupling between the cardiac implant and the sub-cutaneous implant also has a linear relation with distance. The path-loss model is given by the following equation:

$$z = B*x + z(1) \qquad (2),$$

where z is the coupling in dB, A is the slope of the equation in dB per cm, x is the distance in cm and z(1) is the maximum coupling at a distance of 1 cm.

The experimental results show that B is -4.1 dB/cm which means that the coupling reduces at a rate of 4.1 dB with increase in distance between the implants by each cm. The maximum coupling z(1) is recorded as -37.2 dB.

The path-loss between the implant and the off-body antenna is a logarithmic function (see Fig. 7). It is given by the following equation:

$$v = C*10log(x) + v(1) \qquad (3),$$

where v is the coupling in dB, C is the logarithmic decay rate in dB per cm, x is the distance in cm and v(1) is the maximum coupling at a distance of 1 cm.

The experimental results shows that C is -1.4 dB/cm. The maximum coupling v(1) is recorded as -68.4 dB. The coupling decreases logarithmically with distance as generally seen in the case of free space path-loss of RF signals. Free-space path-loss can be imagined as a signal spreading out from the transmitter in the form of a sphere. The intensity of signal decreases with the increase in the surface area of the sphere obeying the laws of conservation of energy. The rate of signal loss is higher in the near-field compared to the far field. The idealized condition will be to determine the pathloss models for the near-field and far-field separately, but it is challenging to determine the exact separation boundary between the near-field and the far-field as the transmitter capsule along with the phantom solution acts as the single radiating antenna in this scenario.

For the implant to off-body antenna communication, the path-loss is dominated by this free-space loss compared to the linear material loss due to the homogeneous heart phantom as the position of the capsule inside the liquid phantom was fixed. Whereas, in case of in-body implant to implant communication, the material loss is highly dominant. The total path-loss model is linear inside the phantom solution and logarithmic in the free space.

Living animal experiments are used to obtain the coupling at few discrete points. Since, it is difficult to maneuver the implants inside the pig to obtain multiple desirable distances to obtain a complete path-loss model, a few recordings are done to compare with the phantom experiment results. For the cardiac implant to implant communication, we obtain a coupling of -74.57 dB and -81.15 dB at 8 cm and 10 cm, respectively. These results are lower than the phantom results by 5.97 dB and 6.95 dB, respectively. For the cardiac implant to sub-cutaneous implant communication, we obtained a coupling of -82.37 dB and -88.31 dB at 12 cm and 13 cm, respectively. These results are lower than the phantom results by 3.23 dB and 3.39 dB respectively.

There is a difference between the phantom and animal experiment results as the animal body is a heterogeneous medium consisting of different tissues as compared to the homogeneous nature of the phantom. For cardiac implant to implant communication, it is observed that the coupling is more in case of phantom experiments compared to the animal experiment because the heart mainly consists of blood which is a highly lossy medium compared to the homogeneous phantom built from average heart tissue properties. Moreover, the movement of the heart during cardiac cycle contributes to the change in the received signal strength. For the link between the heart implant and the sub-cutaneous implant, it is noticed that the coupling is more in case of animal experiments compared to the phantom one. This is due to the presence of empty spaces and low water content tissues like bones in between the cardiac implant and the sub-cutaneous implant placed inside the shoulder in case of the animal experiment.

For the off-body communication, the coupling is -86.2 at 11 cm in the animal experiment in comparison to -83 dB at the same distance in case of the phantom experiment. The results show that the animal experiments closely match with the phantom experiment results.

V. Conclusion and Future Works

The in-body and off-body channel models are presented in this letter for the development of multi-node leadless pacemaker technology. The phantom experiments are in good agreement with the living experiment results. The received signal from the animal experiment is subjected to time-varying shadowing, reflection, and diffraction due to the heart movements during the cardiac cycle which results in a small variation from the phantom experiment results. The future work would involve designing a phantom model replicating the movements during cardiac cycle. Further experiments would facilitate design of a complete prototype of the multi-node leadless capsule pacemaker technology.

1536-1225 (c) 2018 IEEE. Personal use is permitted, but republication/redistribution requires IEEE permission. See http://www.ieee.org/publications_standards/publications/rights/index.html for more information.

This article has been accepted for publication in a future issue of this journal, but has not been fully edited. Content may change prior to final publication. Citation information: DOI 10.1109/LAWP.2018.2878950, IEEE Antennas and Wireless Propagation Letters

ACKNOWLEDGMENT

This work was funded by the European Union's H2020: MSCA: ITN program for the "Wireless In-body Environment Communication – WiBEC" project under the grant agreement no. 675353.

REFERENCES

[1] P. M. Jacobson, "Leadless cardiac pacemaker." U.S. Patent No. 9,358,400, issued Jun. 7, 2016.

[2] C.-P. Lau, et al., "Implantation and Clinical Performance of an Entirely Leadless Cardiac Pacemaker," *International Journal of Heart Rhythm*, vol. 1, no. 1, p. 50, Sep. 2016.

[3] E. H. Nichols and P. Ritter, "Micra Transcatheter Pacing System Safe, Effective," *MD Conference Express*, vol. 15, no. 22, pp. 8–9, Jan. 2015.

[4] S. Sideris, et. al., "Leadless Cardiac Pacemakers: Current status of a modern approach in pacing," *Hellenic Journal of Cardiology*, vol. 58, no. 6, pp. 403–410, May 2017.

[5] K. Takizawa, et. al., "Channel models for wireless body area networks," *2008 30th EMBC*, pp. 1549-1552,Aug. 2008.

[6] Li, Z. Nie, Y. Liu, L. Wang and Y. Hao, "Characterization of In-Body Radio Channels for Wireless Implants", *IEEE Sensors Journal*, vol. 17, no. 5, pp. 1528-1537, Mar. 2017.

[7] P. Bose, A. Khaleghi, M. Albatat, J. Bergsland and I. Balasingham, "RF Channel Modeling for Implant to Implant Communication and Implant to Sub-Cutaneous Implant Communication for Future Leadless Cardiac Pacemakers", *IEEE Transc. on Biomedical Engg*., Mar. 2018 (in press).

[8] A. Khaleghi and I. Balasingham, "Wireless communication link for capsule endoscope at 600 MHz," *2015 37th Annual International Conference of the IEEE Engineering in Medicine and Biology Society (EMBC)*, pp. 4081-4084, Aug. 2015.

[9] A. Khaleghi, I. Balasingham and J. Bergsland, "Medical Implant with Wireless communications", US Patent No. GB201612175D0, Nov. 2017.

[10] A. Khaleghi, I. Balasingham, and R. Chavez-Santiago, "An ultra-wideband wire spiral antenna for in-body communications using different material matching layers," *2014 36th Annual International Conference of the IEEE Engineering in Medicine and Biology Society*, pp. 6985-6988, Aug. 2014.

[11] S. Castello-Palacios, et al., "Formulas for easy-to-prepare tailored phantoms at 2.4 GHz ISM band," *2017 11th International Symposium on Medical Information and Communication Technology (ISMICT)*, pp. 27-31, Feb. 2017.

1536-1225 (c) 2018 IEEE. Personal use is permitted, but republication/redistribution requires IEEE permission. See http://www.ieee.org/publications_standards/publications/rights/index.html for more information.